Published in final edited form as:

Acc Chem Res. 2018 March 20; 51(3): 778–788. doi:10.1021/acs.accounts.7b00635.

Radiolabeling Silica-Based Nanoparticles via Coordination Chemistry: Basic Principles, Strategies, and Applications

Dalong Ni[†], **Dawei Jiang**[†,‡], **Emily B. Ehlerding**[†], **Peng Huang**[‡,*], and **Weibo Cai**[*,†]

[†]Departments of Radiology, Medical Physics, Biomedical Engineering, Materials Science & Engineering, and Pharmaceutical Sciences (Drug Delivery Core), University of Wisconsin Madison, Madison, Wisconsin 53705, United States

[‡]Guangdong Key Laboratory for Biomedical Measurements and Ultrasound Imaging, Laboratory of Evolutionary Theranostics, School of Biomedical Engineering, Health Science Center, Shenzhen University, Shenzhen 518060, China

CONSPECTUS

As one of the most biocompatible and well-tolerated inorganic nanomaterials, silica-based nanoparticles (SiNPs) have received extensive attention over the last several decades. Recently, positron emission tomography (PET) imaging of radiolabeled SiNPs has provided a highly sensitive, noninvasive, and quantitative readout of the organ/tissue distribution, pharmacokinetics, and tumor targeting efficiency in vivo, which can greatly expedite the clinical translation of these promising NPs. Encouraged by the successful PET imaging of patients with metastatic melanoma using ^{124}I-labeled ultrasmall SiNPs (known as Cornell dots or C dots) and their approval as an Investigational New Drug (IND) by the United States Food and Drug Administration, different radioisotopes (^{64}Cu, ^{89}Zr, ^{18}F, ^{68}Ga, ^{124}I, etc.) have been reported to radiolabel a wide variety of SiNPs-based nanostructures, including dense silica ($dSiO_2$), mesoporous silica (MSN), biodegradable mesoporous silica (bMSN), and hollow mesoporous silica nano-particles (HMSN). With in-depth knowledge of coordination chemistry, abundant silanol groups (–Si–O–) on the silica surface or inside mesoporous channels not only can be directly used for chelator-free radiolabeling but also can be readily modified with the right chelators for chelator-based labeling. However, integrating these labeling strategies for constructing stably radiolabeled SiNPs with high efficiency has proven difficult because of the complexity of the involved key parameters, such as the choice of radioisotopes and chelators, nanostructures, and radiolabeling strategy.

In this Account, we present an overview of recent progress in the development of radiolabeled SiNPs for cancer theranostics in the hope of speeding up their biomedical applications and potential translation into the clinic. We first introduce the basic principles and mechanisms for

[*]Corresponding Authors: peng.huang@szu.edu.cn., wcai@uwhealth.org.

ORCID

Dalong Ni: 0000-0001-6679-5414

Dawei Jiang: 0000-0002-4072-0075

Peng Huang: 0000-0003-3651-7813

Weibo Cai: 0000-0003-4641-0833

Author Contributions

D.N. and D.J. contributed equally to this work.

The authors declare no competing financial interest.

radiolabeling SiNPs via coordination chemistry, including general rules of selecting proper radioisotopes, engineering silica nanoplatforms (e.g., $dSiO_2$, MSN, HMSN) accordingly, and chelation strategies for enhanced labeling efficiency and stability, on which our group has focused over the past decade. Generally, the medical applications guide the choice of specific SiNPs for radiolabeling by considering the inherent functionality of SiNPs. The radioisotopes can then be determined according to the amenability of the particular SiNPs for chelator-based or chelator-free radiolabeling to obtain high labeling stability in vivo, which is a prerequisite for PET to truly reflect the behavior of SiNPs since PET imaging detects the isotopes rather than nanoparticles. Next, we highlight several recent representative biomedical applications of radiolabeled SiNPs including molecular imaging to detect specific lesions, PET-guided drug delivery, SiNP-based theranostic cancer agents, and clinical studies. Finally, the challenges and prospects of radiolabeled SiNPs are briefly discussed toward clinical cancer research. We hope that this Account will clarify the recent progress on the radiolabeling of SiNPs for specific medical applications and generate broad interest in integrating nanotechnology and PET imaging. With several ongoing clinical trials, radiolabeled SiNPs offer great potential for future patient stratification and cancer management in clinical settings.

Graphical Abstract

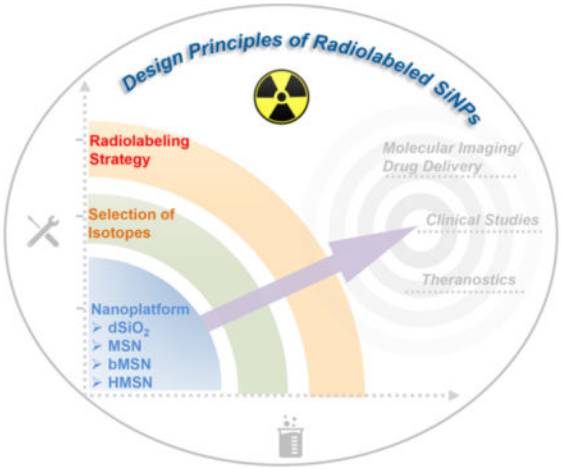

1. INTRODUCTION

Silica-based nanoparticles (SiNPs) have been widely applied as drug delivery systems, imaging nanoprobes, and multifunctional therapeutic nanoplatforms due to the good biocompatibility of silica, which is an endogenous substance, found mainly in bones and “Generally Recognized As Safe” by the United States Food and Drug Administration.[1–5] However, the lack of a real-time detection method to understand the ADME (absorption, distribution, metabolism, and excretion) patterns of SiNPs remains a major challenge for speeding up their potential clinical translation. As a highly sensitive and noninvasive nuclear imaging technique, positron emission tomography (PET) is widely used for preclinical and clinical imaging of diseases with the administration of radiotracers.[6,7] Radio-labeling of SiNPs with radionuclides may provide real-time and quantitative ADME profiles of SiNPs

to evaluate their transportation throughout the body and uptake/retention at target sites. In 2014, Bradbury and co-workers reported a first-in-human clinical trial of ^{124}I-labeled ultrasmall SiNPs (known as Cornell dots or C dots) in metastatic melanoma patients,[8] which instills great confidence in the clinical translation of radiolabeled SiNPs and has accelerated the development of this field.

Since then a significant amount of effort has been devoted to radiolabel SiNPs via various coordination chemistry. The chemically active surface of SiNPs can be readily modified to introduce various functional groups via silanization, thus further conjugating chelators for chelator-based radiolabeling.[9–11] Another simple yet reliable chelator-free labeling technique has also been widely investigated and developed for constructing intrinsically radiolabeled SiNPs by exploiting the strong coordination bond between radiometals and the electron donors (e.g., oxygen, sulfur, or nitrogen atoms) on SiNP nanostructures.[12–14] Meanwhile, the straightforward and precise control of the size, morphology, and composition of SiNPs allow for a comprehensive selection of silica-based platforms, including dense silica (dSiO_2), mesoporous silica (MSN) or biodegradable mesoporous silica (bMSN), and hollow mesoporous silica (HMSN) nanoparticles, enabling the construction of multifunctional nanoplatforms for PET image-guided drug delivery and cancer therapy.

This Account provides an overview of radiolabeled SiNPs with a focus on the basic principles, coordination mechanisms, and design strategies of radiolabeling SiNPs, and briefly introduces their biomedical applications in molecular imaging, image-guided drug delivery, combined cancer therapy, and clinical studies. By elucidating these general concepts and radiochemical structure–function relationships, we hope to provide useful insights into the optimized engineering of radiolabeled SiNPs for their future clinical translation and cancer patient management.

2. DESIGN PRINCIPLES OF RADIOLABELED SiNPs

2.1. Coordination Chemistry

The labeling of SiNPs with radiometals forms a coordination complex, which is the product of a Lewis acid–base reaction. A central radiometal atom (or cation) is coordinated by the neutral molecules or anions (called ligands) by coordination bonds. Ligands are Lewis bases containing at least one pair of electrons to donate to Lewis acids (radioactive metal ions in this case). The affinity between the Lewis base and acid is the key factor that influences the radiolabeling efficiency and stability. On the one hand, SiNPs can be easily surface-engineered with various types of chelators to coordinate radiometals. On the other hand, the inherent abundance of oxygens thus makes SiNPs intrinsic hard Lewis bases for the coordination of hard radiometals (e.g., $^{89}Zr^{4+}$).[12] These basic principles have been widely recognized and applied for successful radiolabeling of SiNPs, under the guidance of which, the selection of silica nanoplatforms, radiometals, and radiolabeling strategies should follow (Figure 1).

2.2. Silica Nanoplatforms

The well-defined siloxane chemistry has enabled construction of silica nanoplatforms with tunable sizes, morphologies, and porosity (dense, mesoporous, hollow, etc.).[3,15] To date, many types of SiNPs have been radiolabeled for PET imaging and image-guided drug delivery or cancer therapy, including $dSiO_2$, MSN or bMSN, and HMSN. Recently, the newer-generation $dSiO_2$-based Cornell prime dots (called C' dots) have been reported, radiolabeled with ^{124}I or ^{89}Zr for tumor PET imaging.[16–18] Besides the ultrasmall C' dots, 20–25 nm sized, near-infrared dye-loaded, and ^{64}Cu-labeled $dSiO_2$ NPs have also been applied for optical/PET dual-modality imaging of sentinel lymph nodes.[11]

With their tunable mesoporous structure, large pore volume, and high surface area, MSNs as drug delivery systems have shown significant advantages over traditional drug nano-carriers.[2,5,19–22] Our group radiolabeled uniform MSNs with well-defined pore sizes with ^{64}Cu for PET imaging through the use of NOTA (1,4,7-triazacyclononane-1,4,7-triacetic acid) and performed image-guided doxorubicin delivery in 4T1 breast cancer model (Figure 2a–c). Systematic in vivo tumor targeting studies in 4T1 tumor-bearing mice clearly demonstrated that ^{64}Cu-NOTA-MSN-TRC105 could accumulate at tumor tissues via both TRC105-mediated binding to tumor vasculature and the enhanced permeability and retention (EPR) effect (Figure 2d).[9] Subsequently, various isotopes ranging from very short-lived ^{18}F to longer-lived ^{89}Zr have also been successfully used for radiolabeling MSNs with appropriate chelators.[23,24] Meanwhile, surface modified HMSNs of different sizes with enhanced drug loading capability were also reported to be radiolabeled with ^{64}Cu or ^{89}Zr for PET imaging and image-guided enhanced drug delivery or combination therapy.[25–28]

2.3. Selection of Radioisotopes

Ideally, the imaging characteristics, decay half-life, and accessibility of radionuclides should be considered to choose an appropriate isotope for the radiolabeling of SiNPs. To avoid a loss of spatial resolution and obtain high-contrast images with less scan time, isotopes with low positron energy and high β^+ decay branching ratio are preferred for PET imaging.[29] Compared to short-lived isotopes, long-lived isotopes are more suitable for transportation and are more flexible for complicated radiolabeling procedures. To date, with continuous endeavors by our laboratory and many other groups, a wide range of isotopes have been reported to successfully radiolabel SiNPs, including short-lived isotopes such as ^{68}Ga, ^{18}F, and ^{45}Ti, and longer-lived isotopes such as ^{124}I, ^{89}Zr, and ^{72}As (Table 1). For diagnostic purposes, the physical half-life of selected isotopes should match the blood circulation half-life of SiNPs to provide a perfect balance of time for monitoring and radiation dose absorbed. Additionally, this may also allow enough time for clearance of background activity to obtain more accurate images. To investigate the biological fate of administered SiNPs, longer-lived isotopes are preferred to evaluate their metabolic and clearance profiles over several days or weeks.

The selection of radioisotopes was compared by Shaffer et al. among six medically important radioisotopes (i.e., ^{89}Zr, ^{68}Ga, ^{111}In, ^{90}Y, ^{177}Lu, and ^{64}Cu), using the $dSiO_2$ as a general substrate.[14] Labeling yields greater than 99% could be obtained for all radioisotopes, and the binding stability was found to be correlated with hardness and oxophilicity of

radioisotopes. Thus, researchers can use this same method to generate radiolabeled SiNPs according to their needs. For example, ^{89}Zr, ^{64}Cu or ^{68}Ga-labeled SiNPs are versatile imaging platforms, while SiNPs labeled with therapeutic isotopes (such as ^{90}Y and ^{177}Lu) may allow for image-guided radiotherapy.

2.4. Radiolabeling Strategies

The radiolabeling strategy is another important factor that must be considered to construct stably labeled SiNPs. An ideal radiolabeling strategy should be easy, fast, robust, and highly efficient and must make only minimal changes to the original properties of SiNPs. Currently, two major methods have been generally used to radiolabel SiNPs with radiometals: chelator-based or chelator-free radiolabeling. It should, however, be noted that exogenous chelators can currently only coordinate with certain radioisotopes. For example, tyrosine residues are usually used for ^{124}I labeling of C or C' dots, and NOTA has been commonly used as the chelator to coordinate ^{64}Cu while DFO (desferrioxamine B) usually chelates ^{89}Zr. Effective chelator-based radiolabeling requires the selection of the best chelator for the isotope of interest. However, some isotopes such as ^{69}Ge, ^{45}Ti, and ^{72}As, are still in search of their perfect chelator or suitable radiolabeling methodology (e.g., for the nonmetal radioisotopes).

Much recent research has focused on developing more reliable chelator-free radiolabeling strategies, which can offer easier, faster, and more general radiolabeling possibilities. For this purpose, our group has reported a chelator-free labeling strategy based on the strong binding of a hard Lewis acid–base pair: ^{89}Zr and oxygen from the deprotonated silanol groups located in the mesoporous pores or on the surface of MSNs.[12] In vivo PET imaging results indicated prominent accumulation of $dSiO_2$ and MSNs in the reticuloendothelial system organs of the liver and spleen (Figure 3a), a general feature observed in many nanomaterial studies which needs to be avoided for future clinical applications. Obvious bone uptake was found for ^{89}Zr-$dSiO_2$ at 24 h postinjection (p.i.), while minimal bone uptake was observed for ^{89}Zr-MSNs up to 21 days p.i. (Figure 3b), indicating a pivotal role of mesopores in stabilizing $^{89}Zr^{4+}$ inside the MSNs. Other types of hard Lewis acid ions such as $^{68}Ga^{3+}$ and $^{45}Ti^{4+}$ were also reported to be easily and efficiently labeled on SiNPs in a chelator-free fashion, further verifying the aforementioned binding principle.[32,33]

However, another widely employed PET isotope, ^{64}Cu, is a softer radiometal that does not stably bind to SiNPs, and NOTA is usually required to construct stable ^{64}Cu-SiNPs. Recently, Grimm and co-workers developed another chelator-free labeling strategy by functionalizing SiNPs with soft electron-donating thiol groups to allow straightforward and stable attachment of ^{64}Cu (Figure 3d).[13] The sulfur-SiNPs showed significantly higher labeling stability compared with native SiNPs based on both EDTA challenge (intact ^{64}Cu: 90.9 ± 5.8% versus 34.9 ± 5.8%) and serum stability studies (intact ^{64}Cu: 93.0 ± 3.6% versus 14.8 ± 3.4%) over 24 h. This approach greatly improved the labeling stability and can be applied for other softer radiometals with an affinity for sulfur. For example, sulfur-avid ^{72}As has been reported by our group to successfully bind to thiolated MSNs.[31,34] Thus, chelator-free radiolabeling of SiNPs can be successfully performed with a wide range of hard (e.g., ^{89}Zr, ^{68}Ga, and ^{45}Ti) and soft (e.g., ^{64}Cu, ^{72}As) radioisotopes with excellent radiolabeling stability.

Besides in vitro chelator-based or chelator-free labeling, in vivo radiolabeling strategy of SiNPs was developed by Lee et al. based on a bioorthogonal reaction, which could successfully overcome some limitations of short-lived radioisotopes (e.g., ^{18}F), such as harsh reaction conditions with complicated and time-consuming labeling procedures.[23] The aza-dibenzocy-clooctyne (DBCO)-functionalized SiNPs first accumulated in the tumor site by the EPR effect, and then rapidly reacted with a subsequently injected ^{18}F-labeled azide synthon (Figure 3e). In vivo PET imaging showed that the ^{18}F-labeled azide radiotracer had significantly higher tumor uptake in mice preinjected with DBCO-SiNPs than that without preinjection, demonstrating the feasibility of radiolabeling with short-lived isotopes in a living system.

3. APPLICATIONS OF RADIOLABELED SILICA-BASED NANOPARTICLES

Over the past few years, many reviews have summarized SiNPs with different nanostructures (e.g., $dSiO_2$, MSN, HMSN, etc.) for applications in drug delivery,[2,21] biomedical imaging,[3] regenerative medicine,[4] and theranostics.[1] In this Section, we will outline the medical applications of radiolabeled SiNPs by exploiting the above-mentioned-radiolabeling principles. Most importantly, the choice of proper SiNPs for radiolabeling is primarily based on the specific intended applications, and should consider the following factors: inherent functionality, surface characteristics for labeling or conjugation, hydrodynamic diameter, and the ability to add diagnostic or therapeutic agents, among other considerations. The diagnostic or therapeutic radioisotopes can then be determined according to the amenability of SiNPs for chelator-based or chelator-free radiolabeling strategies. The decay half-life, labeling reliability, and accessibility of isotopes should also be considered to optimize the medical applications. Moreover, the entire radioactivity handling process should strictly adhere to the “as low as reasonably achievable (ALARA)” guidelines.

3.1. Molecular Imaging

PET imaging is one of the most sensitive molecular imaging techniques that can enable the quantitative visualization of biointeractions between physiological targets and ligands.[29] With simple surface engineering, radiolabeled SiNPs can be further conjugated with various targeting ligands for molecular imaging. These SiNPs should usually be modified with targeting ligands before radiolabeling to obey the ALARA rules.[9,28,35] In this case, due to the addition of biomolecules, the radiolabeling method selected will need to be mild (e.g., temperature and pH value), avoiding any targeting capability loss of the conjugated ligand on the surface of SiNPs.

Recently, Chen et al. reported the successful detection of integrin-expressing lesions in a preclinical model of human melanoma by linking the ultrasmall $dSiO_2$-based C' dots with cRGDY peptides,[17,18] followed by chelator-free or chelator-based radiolabeling of ^{89}Zr (Figure 4a). The only major difference between the chelator-free and the chelator-based ^{89}Zr-cRGDY-PEG-C' dots was the lower in vivo labeling stability and higher (2–4 fold) bone uptake of the former.[18] In another study, Cheng and co-workers developed aptamer-functionalized SiNPs for targeted PET imaging of lymph nodes (LNs) accompanying metastatic tumors.[11] The ^{64}Cu labeled SiNPs were decorated with a 26-mer G-rich DNA

aptamer, which has a high binding affinity for nucleolin overexpressed on breast cancer cells. PET imaging showed that the uptake of the aptamer-functionalized SiNPs in metastatic LNs was significantly enhanced compared to the nontargeted group.

As one of the hallmarks of cancer, angiogenesis plays a key role in tumor growth and metastasis.[36,37] We recently documented the use of ^{64}Cu-MSN-VEGF$_{121}$ for PET imaging targeting the vascular endothelial growth factor receptor (VEGF).[38] Since tumor vasculature also overexpresses CD105, the anti-CD105 antibody, TRC105, or its fragments have been successfully conjugated to ^{64}Cu or ^{89}Zr-labeled SiNPs by our group for molecular imaging.[9,28,35,39,40] These results highlighted the potential of functionalized SiNPs for vasculature targeting, which may allow for better therapeutic outcomes in the future.

3.2. PET-Guided Drug Delivery

Noninvasive PET imaging of angiogenesis and PET-guided antiangiogenic drug delivery may permit cancer diagnosis much earlier and thus allow for better prognoses. An anti-CD105 antibody was successfully conjugated to ^{89}Zr-labeled bMSN for PET-guided drug delivery (Figure 4b), the mesopores of which were designed to carry both small and macromolecular drugs.[39] High tumor accumulation of 11.4 ± 2.1%ID/g at around 6 h p.i. was realized under PET imaging (Figure 4c). Enhanced CD105-targeted delivery of a hydrophobic antiangiogenic drug (e.g., sunitinib malate) and biodegradation of bMSN was also demonstrated, suggesting that such bMSNs can be biodegraded in vivo over time after delivering the drugs to the tumor site. It is worth mentioning that the biodegradation of bMSNs is accompanied by the release of free isotopes, and future studies should aim to properly control the degradation rate and time to reduce the signal background at time of diagnosis or nonspecific toxicity caused by the released diagnostic or therapeutic radionuclides after biodegradation of SiNPs.

To increase the drug loading capacity and enhance drug delivery to tumor sites, TRC105 was conjugated to ^{64}Cu-HMSNs with a large interior cavity for CD105-targeted PET imaging and enhanced drug delivery (Figure 5a).[28] With a large interstitial cavity and a mesoporous shell, up to 1129.2 mg of doxorubicin (DOX) per gram of HMSN could be loaded, which is 3–15 times higher than that reported for normal MSNs (Figure 5b). Subsequently, in vivo enhanced doxorubicin delivery was also demonstrated in 4T1 tumor-bearing mice (Figure 5c). The PET imaging results showed that highest tumor uptake of ^{64}Cu-HMSN-TRC105 was nearly 2 times of that for our previously reported ^{64}Cu-MSN-TRC105 (Figure 5d).[9]

3.3. Cancer Theranostics

Our group has recently developed a variety of multifunctional nanoplatforms based on radiolabeled SiNPs as cancer theranostics for image-guided therapy to optimize therapeutic efficacy. For example, ^{64}Cu was stably labeled on copper sulfide (CuS) NP-coated MSN shells with TRC105 conjugation for tumor vascular targeting and PET imaging-guided photo-thermal therapy (PTT) (Figure 6a).[40] Recently, we also self-assembled ultrasmall CuS NPs on the surface of ^{89}Zr-HMSN to construct core–satellite nanoconstructs (CSNC), and loaded them with porphyrin molecules for multimodal image-guided therapy (Figure 6b).[26] The labeled ^{89}Zr could be used for PET and Cerenkov radiation energy transfer (CRET)

imaging by intrinsically exciting porphyrin molecules, which also served as dyes for fluorescence imaging. Synergistic interaction between CuS-produced PTT and porphyrin-mediated photodynamic therapy (PDT) resulted in an enhanced on-demand photo-therapeutic effect to completely eliminate the tumor (Figure 6c). Future studies should focus on simplifying the synthetic process of the nanostructures, making them easier for clinical translation.

In another study, the cavity of ^{89}Zr-HMSN was filled with a well-known photosensitizer, chlorin e6 (Ce6), which has a strong absorption band peaking at 400 nm that matches well with the Cerenkov radiation from ^{89}Zr (Figure 6d).[25] The transferred energy of Cerenkov radiation could activate Ce6 molecules nearby, generating toxic reactive oxygen species to trigger PDT in tumor cells. Without using any external light source, tumor growth in mice injected with ^{89}Zr-HMSN-Ce6 was completely inhibited within 14 days p.i. (Figure 6e). Such nanoplatforms based on radiolabeled SiNPs with internally triggered PDT could overcome the tissue penetration depth of traditional external light excitation.

3.4. Studies in the Clinic

Radiolabeled SiNPs offer excellent biocompatibility for nuclear imaging, providing guidance for particle design optimization. The $dSiO_2$-based C dots with an inherent fluorescent dye (Cy5), PEG modification, and cRGDY peptide functionalization were radiolabeled with ^{124}I (i.e., ^{124}I-cRGDY–PEG–C dots) for dual-modal optical/PET imaging as the first-in-human clinical study of radiolabeled SiNPs.[8] These ultrasmall C dots exhibited preferential renal clearance with specific tumor accumulation and reduced off-target uptake not only in murine models of melanoma, but also in metastatic melanoma patients (Figure 7). The liver uptake of the patient was very low (~1.28×10^{-3} %ID/g) at 72 h after injection, while the targeting efficiency of C dots remains a concern since only ~0.01% of the injected dose was localized in tumor site. Systematic safety evaluation suggested that no changes were found with respect to the blood and urine profiles and confirmed that C dots did not elicit any adverse effects on the renal and liver functions of patients. Since this is the first report of radiolabeled nanoparticle imaging in humans, the establishment of comprehensive biological profiles (including circulation half-life, biodistribution, pharmacokinetics, and radiation dosimetry) of C dots has greatly deepened our understanding of SiNPs in vivo, which may extend to other types of nanomaterials in the context of cancer diagnosis, management, and therapeutic intervention.[41]

4. CONCLUSIONS AND PROSPECTS

Combining the unique properties of SiNPs and PET imaging represents a synergistic relationship whereby the radiolabeled SiNPs can be readily engineered as effective nanoplatforms for PET molecular imaging, image-guided drug delivery, and theranostics. By in-depth understanding of the basic radio-labeling principles, SiNPs with different nanostructures have been successfully radiolabeled with a variety of isotopes via traditional coordination chemistry. Importantly, the radio-labeled $dSiO_2$-based C or C' dots are currently being investigated as a PET/optical platform for early phase clinical trials.

However, the complexity of clinical translation of radio-labeled SiNPs is much greater than initially expected, calling for concerted collaboration in a multidisciplinary manner among material scientists, chemists, biologists, clinicians, as well as the regulatory agencies. More efforts should be devoted to facilitate the development and expand the medical application of radiolabeled SiNPs for the benefit of patients in the future. First, besides PET/optical dual-modal imaging, another preferred choice is to integrate magnetic resonance imaging (MRI) contrast agents with radiolabeled SiNPs for PET/MRI dual-modal imaging since PET/MRI scanners have become commercially available and are receiving extensive attention.[42–44] Second, radiotherapeutic isotopes (e.g., ^{177}Lu, ^{90}Y) can also be labeled on SiNPs to construct a simplified theranostic platform for simultaneous radiotherapy.[45,46] Lastly, many of research studies reported in the literature were performed on subcutaneous tumor models, and future application of radiolabeled SiNPs should be directed toward the orthotopic tumors as well as patient-derived tumor models, for more clinically relevant information. The basic radiolabeling principles presented in this Account can also be applied to radiolabel other nanomaterial systems,[47,48] moving nano-technology into the clinic to usher in the new era of precision medicine.

Acknowledgments

This work was supported, in part, by the University of Wisconsin—Madison, the National Institutes of Health (NIBIB/NCI T32CA009206, T32GM008505, and P30CA014520), the American Cancer Society (125246-RSG-13-099-01-CCE), the National Natural Science Foundation of China (51573096, 51703132, 31771036, 81401465), and the Basic Research Program of Shenzhen (JCYJ20170412111100742, JCYJ20160422091238319).

References

1. Chen Y, Chen H, Shi J. In vivo bio-safety evaluations and diagnostic/therapeutic applications of chemically designed mesoporous silica nanoparticles. Adv Mater. 2013; 25:3144–3176. [PubMed: 23681931]
2. Tang F, Li L, Chen D. Mesoporous silica nanoparticles: synthesis, biocompatibility and drug delivery. Adv Mater. 2012; 24:1504–1534. [PubMed: 22378538]
3. Vivero-Escoto JL, Huxford-Phillips RC, Lin W. Silica-based nanoprobes for biomedical imaging and theranostic applications. Chem Soc Rev. 2012; 41:2673–2685. [PubMed: 22234515]
4. Perez RA, Singh RK, Kim TH, Kim HW. Silica-based multifunctional nanodelivery systems toward regenerative medicine. Mater Horiz. 2017; 4:772–799.
5. Wu SH, Mou CY, Lin HP. Synthesis of mesoporous silica nanoparticles. Chem Soc Rev. 2013; 42:3862–3875. [PubMed: 23403864]
6. Goel S, England CG, Chen F, Cai W. Positron emission tomography and nanotechnology: A dynamic duo for cancer theranostics. Adv Drug Delivery Rev. 2017; 113:157–176.
7. Sun X, Cai W, Chen X. Positron emission tomography imaging using radiolabeled inorganic nanomaterials. Acc Chem Res. 2015; 48:286–294. [PubMed: 25635467]
8. Phillips E, Penate-Medina O, Zanzonico PB, Carvajal RD, Mohan P, Ye Y, Humm J, Gonen M, Kalaigian H, Schoder H, Strauss HW, Larson SM, Wiesner U, Bradbury MS. Clinical translation of an ultrasmall inorganic optical-PET imaging nanoparticle probe. Sci Transl Med. 2014; 6:260ra149.
9. Chen F, Hong H, Zhang Y, Valdovinos HF, Shi S, Kwon GS, Theuer CP, Barnhart TE, Cai W. In vivo tumor targeting and image-guided drug delivery with antibody-conjugated, radiolabeled mesoporous silica nanoparticles. ACS Nano. 2013; 7:9027–9039. [PubMed: 24083623]
10. Al Faraj A, Alotaibi B, Shaik AP, Shamma KZ, Al Jammaz I, Gerl J. Sodium-22-radiolabeled silica nanoparticles as new radiotracer for biomedical applications: in vivo positron emission tomography imaging, biodistribution, and biocompatibility. Int J Nanomed. 2015; 10:6293–6302.

11. Tang L, Yang X, Dobrucki LW, Chaudhury I, Yin Q, Yao C, Lezmi S, Helferich WG, Fan TM, Cheng J. Aptamer-functionalized, ultra-small, monodisperse silica nanoconjugates for targeted dual-modal imaging of lymph nodes with metastatic tumors. Angew Chem, Int Ed. 2012; 51:12721–12726.
12. Chen F, Goel S, Valdovinos HF, Luo H, Hernandez R, Barnhart TE, Cai W. In Vivo Integrity and Biological Fate of Chelator-Free Zirconium-89-Labeled Mesoporous Silica Nanoparticles. ACS Nano. 2015; 9:7950–7959. [PubMed: 26213260]
13. Shaffer TM, Harmsen S, Khwaja E, Kircher MF, Drain CM, Grimm J. Stable Radiolabeling of Sulfur-Functionalized Silica Nanoparticles with Copper-64. Nano Lett. 2016; 16:5601–5604. [PubMed: 27464258]
14. Shaffer TM, Wall MA, Harmsen S, Longo VA, Drain CM, Kircher MF, Grimm J. Silica nanoparticles as substrates for chelator-free labeling of oxophilic radioisotopes. Nano Lett. 2015; 15:864–868. [PubMed: 25559467]
15. Burns A, Ow H, Wiesner U. Fluorescent core-shell silica nanoparticles: towards Lab on a Particle architectures for nano-biotechnology. Chem Soc Rev. 2006; 35:1028–1042. [PubMed: 17057833]
16. Ma K, Mendoza C, Hanson M, Werner-Zwanziger U, Zwanziger J, Wiesner U. Control of Ultrasmall Sub-10 nm Ligand-Functionalized Fluorescent Core–Shell Silica Nanoparticle Growth in Water. Chem Mater. 2015; 27:4119–4133.
17. Chen F, Ma K, Benezra M, Zhang L, Cheal SM, Phillips E, Yoo B, Pauliah M, Overholtzer M, Zanzonico P, Sequeira S, Gonen M, Quinn T, Wiesner U, Bradbury MS. Cancer-Targeting Ultrasmall Silica Nanoparticles for Clinical Translation: Physicochemical Structure and Biological Property Correlations. Chem Mater. 2017; 29:8766–8779. [PubMed: 29129959]
18. Chen F, Ma K, Zhang L, Madajewski B, Zanzonico P, Sequeira S, Gonen M, Wiesner U, Bradbury MS. Target-or-Clear Zirconium-89 Labeled Silica Nanoparticles for Enhanced Cancer-Directed Uptake in Melanoma: A Comparison of Radiolabeling Strategies. Chem Mater. 2017; 29:8269–8281. [PubMed: 29123332]
19. Meng H, Wang M, Liu H, Liu X, Situ A, Wu B, Ji Z, Chang CH, Nel AE. Use of a lipid-coated mesoporous silica nanoparticle platform for synergistic gemcitabine and paclitaxel delivery to human pancreatic cancer in mice. ACS Nano. 2015; 9:3540–3557. [PubMed: 25776964]
20. Shen D, Yang J, Li X, Zhou L, Zhang R, Li W, Chen L, Wang R, Zhang F, Zhao D. Biphase stratification approach to three-dimensional dendritic biodegradable mesoporous silica nanospheres. Nano Lett. 2014; 14:923–932. [PubMed: 24467566]
21. He Q, Shi J. MSN anti-cancer nanomedicines: chemotherapy enhancement, overcoming of drug resistance, and metastasis inhibition. Adv Mater. 2014; 26:391–411. [PubMed: 24142549]
22. Lu N, Huang P, Fan W, Wang Z, Liu Y, Wang S, Zhang G, Hu J, Liu W, Niu G, Leapman RD, Lu G, Chen X. Tri-stimuli-responsive biodegradable theranostics for mild hyperthermia enhanced chemotherapy. Biomaterials. 2017; 126:39–48. [PubMed: 28254692]
23. Lee SB, Kim HL, Jeong HJ, Lim ST, Sohn MH, Kim DW. Mesoporous silica nanoparticle pretargeting for PET imaging based on a rapid bioorthogonal reaction in a living body. Angew Chem, Int Ed. 2013; 52:10549–10552.
24. Miller L, Winter G, Baur B, Witulla B, Solbach C, Reske S, Linden M. Synthesis, characterization, and biodistribution of multiple 89Zr-labeled pore-expanded mesoporous silica nanoparticles for PET. Nanoscale. 2014; 6:4928–4935. [PubMed: 24675844]
25. Kamkaew A, Cheng L, Goel S, Valdovinos HF, Barnhart TE, Liu Z, Cai W. Cerenkov Radiation Induced Photodynamic Therapy Using Chlorin e6-Loaded Hollow Mesoporous Silica Nanoparticles. ACS Appl Mater Interfaces. 2016; 8:26630–26637. [PubMed: 27657487]
26. Goel S, Ferreira CA, Chen F, Ellison PA, Siamof CM, Barnhart TE, Cai W. Activatable Hybrid Nanotheranostics for Tetramodal Imaging and Synergistic Photothermal/Photodynamic Therapy. Adv Mater. 2018; 30:1704367.
27. Chakravarty R, Goel S, Hong H, Chen F, Valdovinos HF, Hernandez R, Barnhart TE, Cai W. Hollow mesoporous silica nanoparticles for tumor vasculature targeting and PET image-guided drug delivery. Nanomedicine. 2015; 10:1233–1246. [PubMed: 25955122]

28. Chen F, Hong H, Shi S, Goel S, Valdovinos HF, Hernandez R, Theuer CP, Barnhart TE, Cai W. Engineering of hollow mesoporous silica nanoparticles for remarkably enhanced tumor active targeting efficacy. Sci Rep. 2015; 4:5080.
29. Ametamey SM, Honer M, Schubiger PA. Molecular imaging with PET. Chem Rev. 2008; 108:1501–1516. [PubMed: 18426240]
30. Benezra M, Penate-Medina O, Zanzonico PB, Schaer D, Ow H, Burns A, DeStanchina E, Longo V, Herz E, Iyer S, Wolchok J, Larson SM, Wiesner U, Bradbury MS. Multimodal silica nanoparticles are effective cancer-targeted probes in a model of human melanoma. J Clin Invest. 2011; 121:2768–2780. [PubMed: 21670497]
31. Ellison PA, Barnhart TE, Chen F, Hong H, Zhang Y, Theuer CP, Cai W, Nickles RJ, DeJesus OT. High Yield Production and Radiochemical Isolation of Isotopically Pure Arsenic-72 and Novel Radioarsenic Labeling Strategies for the Development of Theranostic Radiopharmaceuticals. Bioconjugate Chem. 2016; 27:179–188.
32. Chen F, Valdovinos HF, Hernandez R, Goel S, Barnhart TE, Cai W. Intrinsic radiolabeling of Titanium-45 using mesoporous silica nanoparticles. Acta Pharmacol Sin. 2017; 38:907–913. [PubMed: 28414201]
33. Burke BP, Baghdadi N, Kownacka AE, Nigam S, Clemente GS, Al-Yassiry MM, Domarkas J, Lorch M, Pickles M, Gibbs P, Tripier R, Cawthorne C, Archibald SJ. Chelator free gallium-68 radiolabelling of silica coated iron oxide nanorods via surface interactions. Nanoscale. 2015; 7:14889–14896. [PubMed: 26292197]
34. Ellison PA, Chen F, Goel S, Barnhart TE, Nickles RJ, DeJesus OT, Cai W. Intrinsic and Stable Conjugation of Thiolated Mesoporous Silica Nanoparticles with Radioarsenic. ACS Appl Mater Interfaces. 2017; 9:6772–6781. [PubMed: 28165700]
35. Chen F, Nayak TR, Goel S, Valdovinos HF, Hong H, Theuer CP, Barnhart TE, Cai W. In vivo tumor vasculature targeted PET/NIRF imaging with TRC105(Fab)-conjugated, dual-labeled mesoporous silica nanoparticles. Mol Pharmaceutics. 2014; 11:4007–4014.
36. Hanahan D, Weinberg RA. Hallmarks of cancer: the next generation. Cell. 2011; 144:646–674. [PubMed: 21376230]
37. Cai W, Chen X. Multimodality molecular imaging of tumor angiogenesis. J Nucl Med. 2008; 49(Suppl2):113S–128S. [PubMed: 18523069]
38. Goel S, Chen F, Hong H, Valdovinos HF, Hernandez R, Shi S, Barnhart TE, Cai W. VEGF(1)(2)(1)-conjugated mesoporous silica nanoparticle: a tumor targeted drug delivery system. ACS Appl Mater Interfaces. 2014; 6:21677–21685. [PubMed: 25353068]
39. Goel S, Chen F, Luan S, Valdovinos HF, Shi S, Graves SA, Ai F, Barnhart TE, Theuer CP, Cai W. Engineering Intrinsically Zirconium-89 Radiolabeled Self-Destructing Mesoporous Silica Nanostructures for In Vivo Biodistribution and Tumor Targeting Studies. Adv Sci. 2016; 3:1600122.
40. Chen F, Hong H, Goel S, Graves SA, Orbay H, Ehlerding EB, Shi S, Theuer CP, Nickles RJ, Cai W. In Vivo Tumor Vasculature Targeting of CuS@MSN Based Theranostic Nanomedicine. ACS Nano. 2015; 9:3926–3934. [PubMed: 25843647]
41. Shi J, Kantoff PW, Wooster R, Farokhzad OC. Cancer nanomedicine: progress, challenges and opportunities. Nat Rev Cancer. 2017; 17:20–37. [PubMed: 27834398]
42. Chakravarty R, Valdovinos HF, Chen F, Lewis CM, Ellison PA, Luo H, Meyerand ME, Nickles RJ, Cai W. Intrinsically germanium-69-labeled iron oxide nanoparticles: synthesis and in-vivo dual-modality PET/MR imaging. Adv Mater. 2014; 26:5119–5123. [PubMed: 24944166]
43. Chen F, Ellison PA, Lewis CM, Hong H, Zhang Y, Shi SX, Hernandez R, Meyerand ME, Barnhart TE, Cai WB. Chelator-Free Synthesis of a Dual-Modality PET/MRI Agent. Angew Chem, Int Ed. 2013; 52:13319–13323.
44. Ni D, Bu W, Ehlerding EB, Cai W, Shi J. Engineering of inorganic nanoparticles as magnetic resonance imaging contrast agents. Chem Soc Rev. 2017; 46:7438–7468. [PubMed: 29071327]
45. Yu B, Wei H, He Q, Ferreira CA, Kutyreff CJ, Ni D, Rosenkrans ZT, Cheng L, Yu F, Engle JW, Lan X, Cai W. Efficient Uptake of (177) Lu-Porphyrin-PEG Nanocomplexes by Tumor Mitochondria for Multimodal-Imaging-Guided Combination Therapy. Angew Chem, Int Ed. 2018; 57:218–222.

46. Goel S, Ni D, Cai W. Harnessing the Power of Nanotechnology for Enhanced Radiation Therapy. ACS Nano. 2017; 11:5233–5237. [PubMed: 28621524]

47. Ni D, Jiang D, Valdovinos HF, Ehlerding EB, Yu B, Barnhart TE, Huang P, Cai W. Bioresponsive Polyoxometalate Cluster for Redox-Activated Photoacoustic Imaging-Guided Photothermal Cancer Therapy. Nano Lett. 2017; 17:3282–3289. [PubMed: 28418679]

48. Cheng L, Shen S, Jiang D, Jin Q, Ellison PA, Ehlerding EB, Goel S, Song G, Huang P, Barnhart TE, Liu Z, Cai W. Chelator-Free Labeling of Metal Oxide Nanostructures with Zirconium-89 for Positron Emission Tomography Imaging. ACS Nano. 2017; 11:12193–12201. [PubMed: 29178789]

Biographies

Dalong Ni received his Ph.D. degree in 2016 from the Shanghai Institute of Ceramics, Chinese Academy of Sciences. He then joined the Department of Radiology at the University of Wisconsin—Madison as a postdoctoral fellow under the supervision of Prof. Weibo Cai, working on the design and synthesis of multifunctional nanoplatforms for imaging and therapy applications.

Dawei Jiang received his Ph.D. degree from Shanghai Institute of Applied Physics, Chinese Academy of Sciences in 2015. He is currently a postdoctoral fellow, working on the design and biomedical applications of radiopharmaceuticals for nuclear medicine and molecular imaging.

Emily B. Ehlerding received her M.S. degree from the UW—Madison in 2016, and her B.S. degree from Manchester University in 2014. She is currently a Ph.D. candidate at UW—Madison, working with antibody-based platforms for multimodality imaging of immunother-apy-related targets.

Peng Huang received his Ph.D. in Biomedical Engineering from the Shanghai Jiao Tong University in 2012 and is now a Distinguished Professor at the Shenzhen University. His research focuses on the design, synthesis, and biomedical applications of activatable theranostics.

Weibo Cai received his Ph.D. degree from University of California San Diego in 2004 and is now an Associate Professor at the UW—Madison (http://mi.wisc.edu). His research is primarily focused on molecular imaging and nanotechnology, investigating the biomedical applications of various agents developed in his laboratory for imaging and therapy of various diseases.

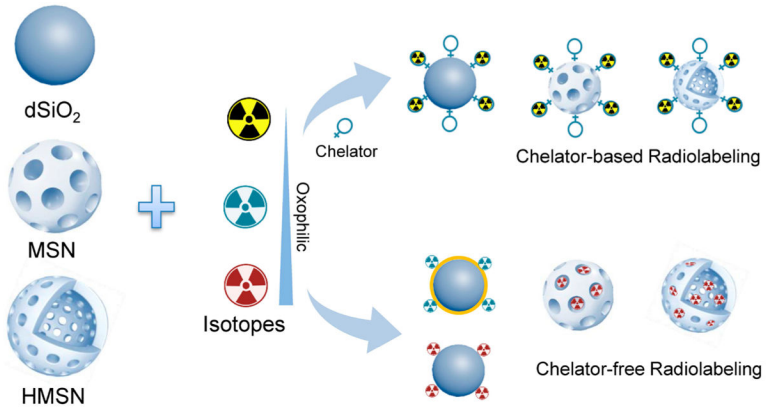

Figure 1.

Schematic illustration of radiolabeling different types of SiNPs such as $dSiO_2$, MSN, and HMSN by chelator-based or chelator-free labeling strategies.

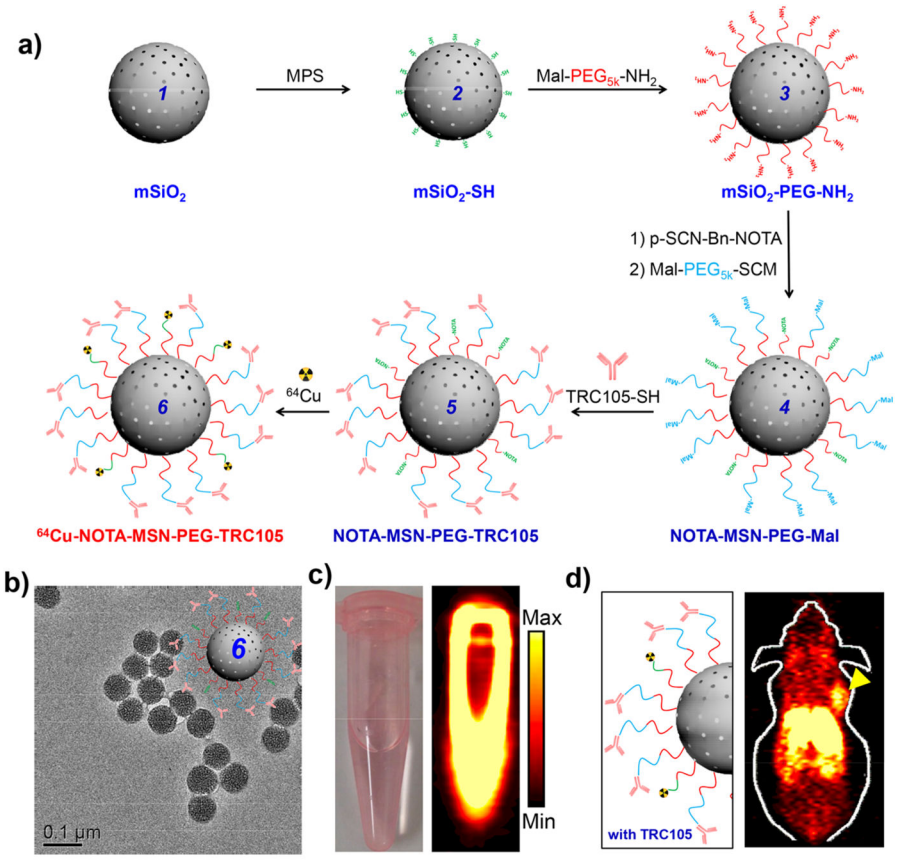

Figure 2.

(a) Schematic illustration of radiolabeling MSN with ^{64}Cu via a chelator-based strategy. (b) TEM image of NOTA-MSN-PEG-TRC105 in PBS solution. (c) Digital photo (left) and a PET phantom image (right) of radiolabeled SiNPs in phosphate-buffered saline (PBS) solution. (d) In vivo CD105-targeted PET imaging of a tumor-bearing mouse. Reproduced with permission from ref 9. Copyright 2013 American Chemical Society.

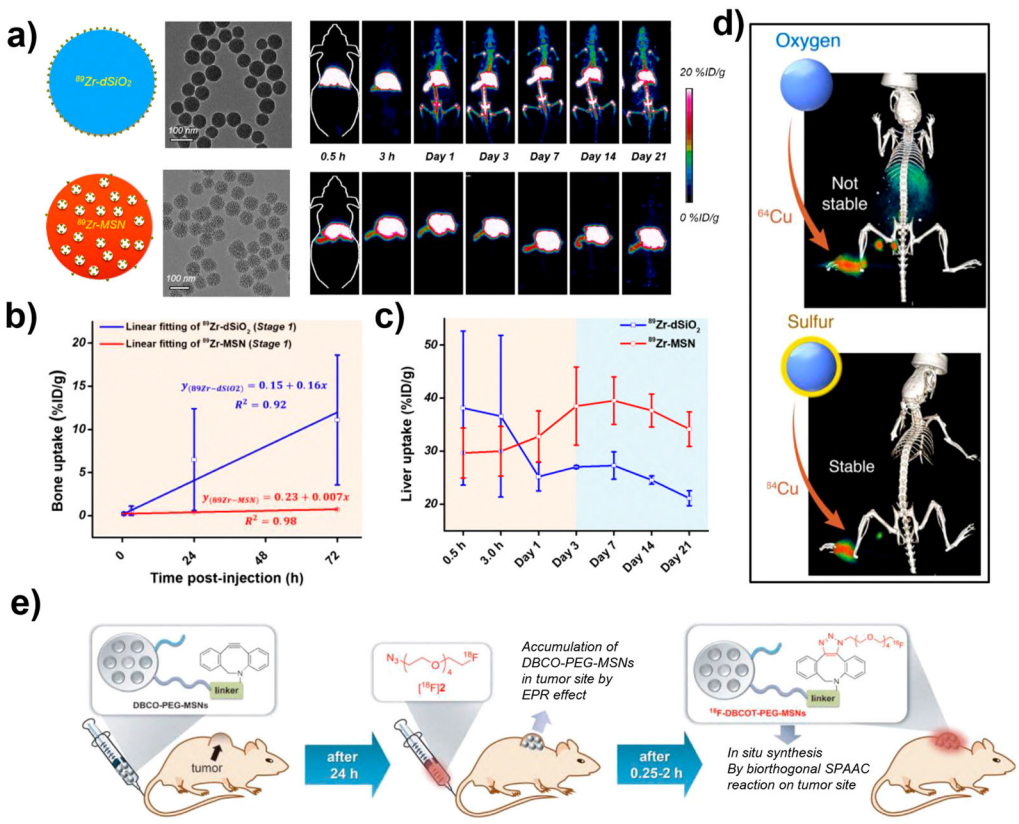

Figure 3.

(a) Schematic illustration, TEM images, and in vivo PET images of mice after i.v. injection of ^{89}Zr-dSiO$_2$ or ^{89}Zr-MSN. (b) Linear fitting of ^{89}Zr in the bone within 72 h postinjection. (c) Time–activity curves of the liver after injection of ^{89}Zr-dSiO$_2$ or ^{89}Zr-MSN over 21 days. Reproduced with permission from ref 12. Copyright 2015 American Chemical Society. (d) ^{64}Cu-sulfur-SiNPs injected into the footpad allowed for lymph node imaging with high stability, whereas ^{64}Cu-SiNPs showed off-target uptake in the liver, spleen, and intestine. Reproduced with permission from ref 13. Copyright 2016 American Chemical Society. (e) Schematic illustration of the in vivo radiolabeling of DBCO-SiNPs with ^{18}F using a bioorthogonal reaction. Reproduced with permission from ref 23. Copyright 2013 Wiley-VCH.

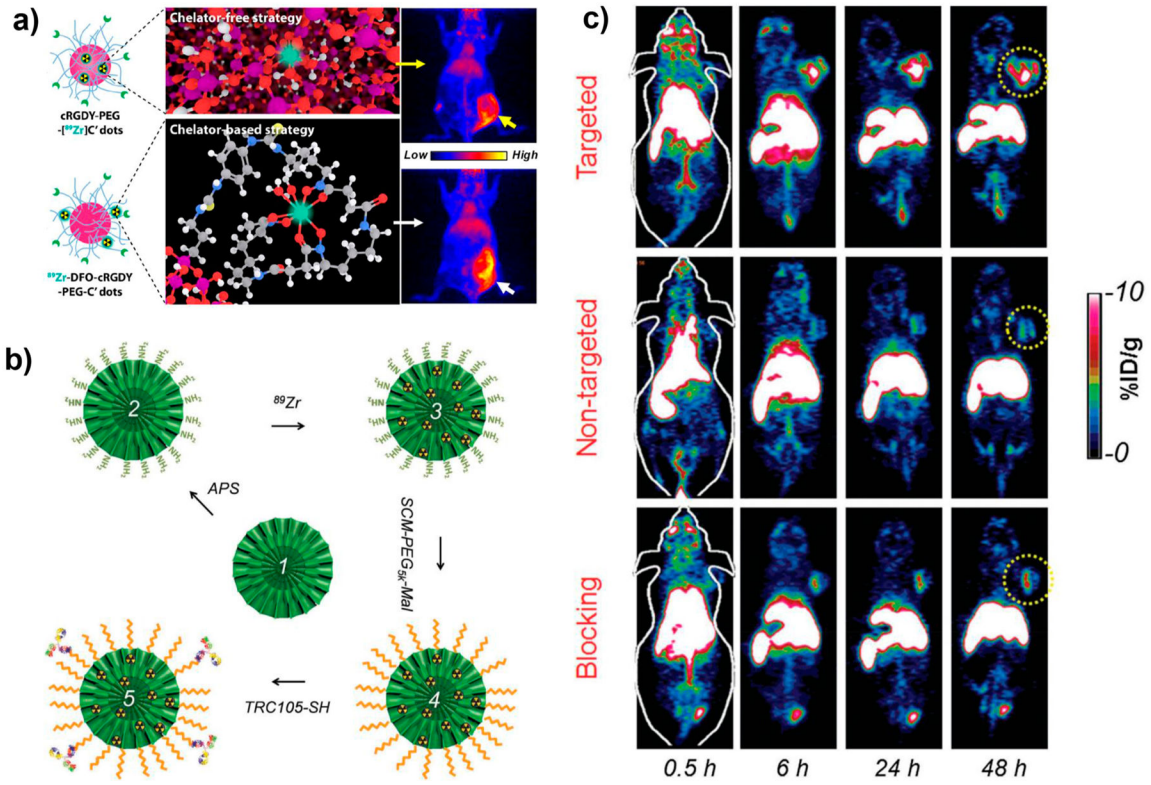

Figure 4.

(a) In vivo targeted PET imaging with chelator-free or chelator-based ^{89}Zr-cRGDY-PEG-C' dots. Reproduced with permission from ref 18. Copyright 2017 American Chemical Society. (b) Schematic depiction of the synthesis of ^{89}Zr-bMSN-TRC105. (c) In vivo PET imaging targeting tumor vasculature using ^{89}Zr-bMSN-TRC105. Yellow circles indicate the location of 4T1 tumors. Reproduced with permission from ref 39. Copyright 2016 Wiley-VCH.

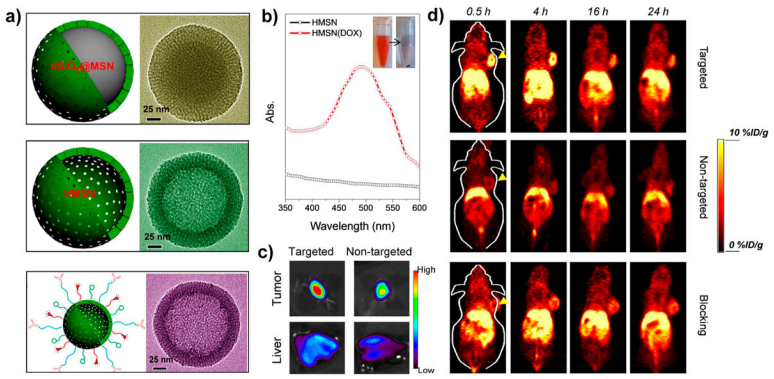

Figure 5.

(a) Schematic (left) and TEM image (right) of single $dSiO_2$@MSN, HMSN, and HMSN-TRC105 NPs. (b) UV–vis spectra of HMSNs with and without DOX in aqueous solution. (c) Ex vivo optical imaging of DOX accumulation in the tumor and liver after intravenous injection of HMSN: targeted, HMSN-TRC105 loaded with DOX; nontargeted, HMSN loaded with DOX. (d) In vivo tumor-targeted PET imaging at different time points p.i. Tumors are indicated by yellow arrowheads. Reproduced with permission from ref 28. Copyright 2015 Nature Publishing Group.

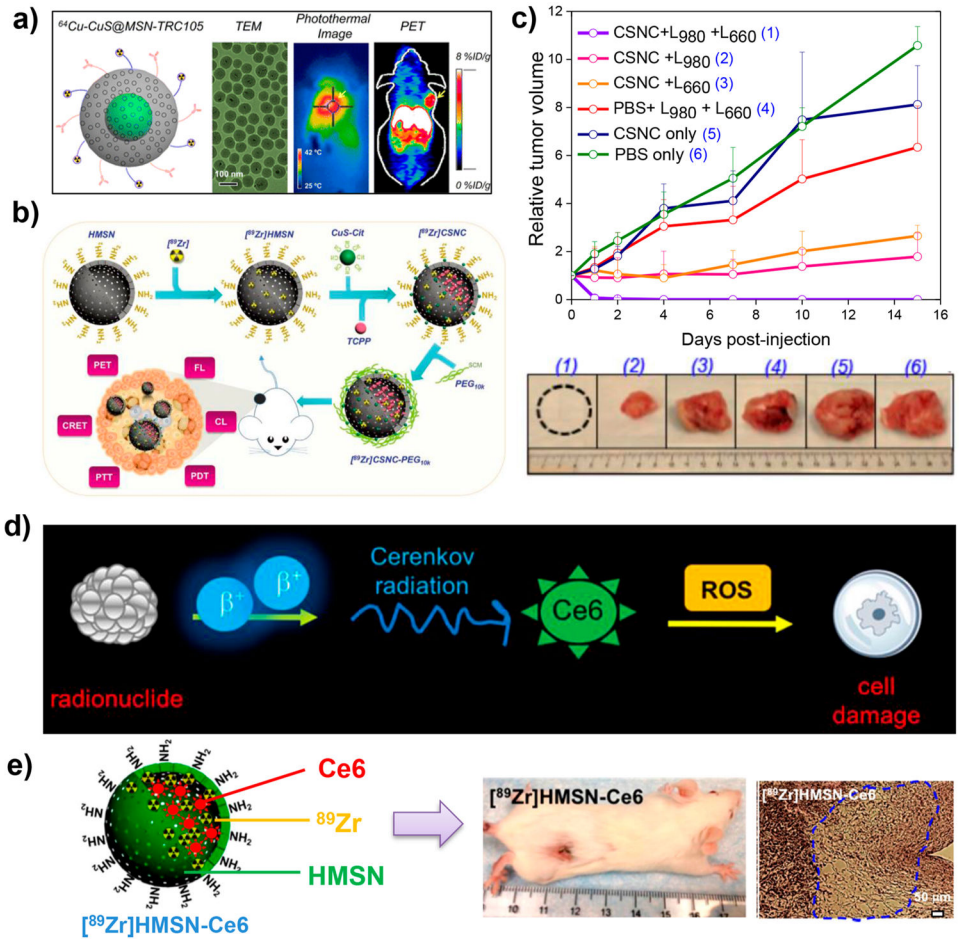

Figure 6.

(a) In vivo tumor vasculature targeting of CuS@MSN. Reproduced with permission from ref 40. Copyright 2015 American Chemical Society. (b) Schematic illustration of the self-assembly of radiolabeled CSNC for multimodal image-guided synergistic photothermal therapy (PTT) and photodynamic therapy (PDT). (c) Time-dependent tumor growth curves after various treatments and digital photographs of tumors explanted from different treatment groups after 15 days. Reproduced with permission from ref 26. Copyright 2018 Wiley-VCH. (d) Schematic illustration of [^{89}Zr]HMSN-Ce6 for Cerenkov radiation-induced PDT. (e) Schematic of [^{89}Zr]HMSN-Ce6 NPs and representative photographs of a tumor-bearing mouse and H&E-stained tumor slice after treatment. Reproduced with permission from ref 25. Copyright 2016 American Chemical Society.

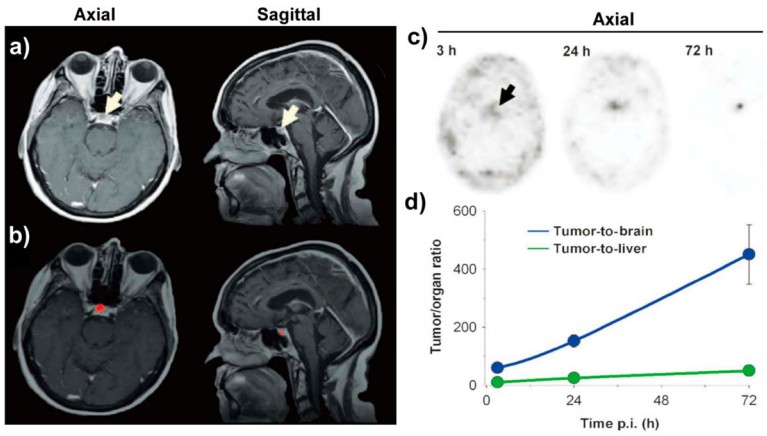

Figure 7.

(a) Multiplanar contrast-enhanced MR axial and sagittal images of a patient with anorectal mucosal melanoma at 72 h p.i. demonstrated a subcentimeter cystic focus (arrows) within the right aspect of the anterior pituitary gland. (b) Co-registered axial and sagittal MRI-PET images reveal increased focal activity (red, ^{124}I-cRGDY–PEG–C dots) localized to the lesion site. (c) Axial PET images of ^{124}I-cRGDY–PEG–C dots in the brain at 3, 24, and 72 h after injection showed progressive accumulation of activity within the sellar region. (D) Tumor-to-brain and tumor-to-liver activity ratios as a function of p.i. time. Reproduced with permission from ref 8. Copyright 2014 American Association for the Advancement of Science.

Table 1

Representative Radiolabeled SiNPs for PET Imaging and Biomedical Applications[a]

SiNPs	isotope	half-life	labeling strategy	application	ref
C dots	^{124}I	4.2 days	chelator-based	molecular imaging	8, 30
C' dots	^{89}Zr	78.4 h	chelator-based/chelator-free	molecular imaging	18
$dSiO_2$	^{64}Cu	12.7 h	chelator-based	imaging of LN metastasis	11
$dSiO_2$	^{89}Zr or ^{68}Ga	78.4 h or 67.7 min	chelator-free	biodistribution/LN imaging	14
$dSiO_2$	^{64}Cu	12.7 h	chelator-free	LN imaging	13
MSN	^{18}F	109.8 min	in vivo labeling	tumor imaging	23
MSN	*As	^{72}As, 26 h	chelator-free	biodistribution	31
MSN	^{45}Ti	3.08 h	chelator-free	tumor imaging	32
MSN	^{64}Cu	12.7 h	chelator-based	molecular imaging/drug delivery	9
MSN	^{89}Zr	78.4 h	chelator-free	biodistribution	12
HMSN	^{64}Cu	12.7 h	chelator-based	molecular imaging/drug delivery	28
HMSN	^{89}Zr	78.4 h	chelator-free	theranostics	25

[a]Note: C dots, Cornell dots; C' dots, Cornell prime dots; $dSiO_2$, dense silica nanoparticles; MSN, mesoporous silica nanoparticles; HMSN, hollow mesoporous silica nanoparticles; LN, lymph node. Molecular imaging, tumor diagnosis based on actively targeted imaging; tumor imaging, tumor diagnosis based on the EPR effect.